

Critical Current Characteristics of $\text{YBa}_2\text{Cu}_3\text{O}_7$ Thin Films on (110) SrTiO_3

Edward J. Cukauskas, Jeffrey M. Pond, *Member, IEEE*, Elizabeth A. Dobisz, and William J. DeSisto

Abstract—The material and electrical characteristics of $\text{YBa}_2\text{Cu}_3\text{O}_7$ (YBCO) thin films deposited by inverted cylindrical magnetron sputtering on (110) SrTiO_3 (STO) were investigated. X-ray diffractometry shows the grain orientations to be predominantly the YBCO (110) and (103) with no evidence of *c*-axis grains. Electron micrographs show the film surface to consist of coupled elongated grains parallel to the (110) STO edge. The films were patterned into small 2.5 mm squares parallel to the substrate edges for electrical characterization. Transport currents parallel and perpendicular to the (110) substrate edge showed a 945:1 anisotropy in film resistance and a factor of two in critical current density for temperatures below 60% of the transition temperature (T_c). The temperature dependence of the critical current near T_c was quadratic-like and strongly dependent on the value of T_c used in the analysis. For the two orientations, there was nearly a 6K difference in T_c as determined by the point at which the critical current became zero. The response of the critical current to small magnetic fields was greater for transport current along the *c*-axis direction and was observable over a temperature interval nearly four times greater than for current along the basal plane. These YBCO thin films have good response to small magnetic fields and are suitable for vortex flow device development.

Index Terms—High-temperature superconductors, microwave measurements, superconducting films, superconducting materials, superconducting materials measurements.

I. INTRODUCTION

THE EXISTENCE of the electrons in the planes and chains of the copper oxide High Temperature Superconductors (HTS) results in an anisotropic material having intrinsic Josephson coupled planes separated by the insulating regions within the unit cell [1], [2]. The study of the transport characteristics in HTS thin films has led to much insight into the understanding of intergranular and intragranular coupling in these materials. The temperature dependence of the critical current in YBCO thin films has been associated with Josephson-like coupling mechanisms [3]–[6]. These mechanisms include *SIS*, *SNS*, and *SINS* coupling, where *S* is a superconductor, *I* is an insulator, and *N* is a normal metal. They affect the transport characteristics of the superconducting film [7]. These films act like large arrays of Josephson coupled grains, where the superconducting grains correspond to the

electrodes of the junction and the material between the grains corresponds to the barrier. This intergranular coupling influences the response of HTS thin films to external radiation and applied magnetic fields. Over the past several years, researchers have measured and reported intrinsic Josephson-like junction current-voltage (*I*–*V*) characteristics in *c*-axis YBCO thin films. These measurements relate the physics of intragranular coupling to the layered microstructure of these materials. Small area mesa structures have been fabricated into YBCO and single crystal $\text{Bi}_2\text{Sr}_2\text{CaCu}_2\text{O}_{8+x}$ films for investigating these intrinsic Josephson junction characteristics [8], [9].

The effects of the layered microstructure of HTS materials are readily observable in both their superconducting and normal state properties. Most evident is the anisotropy in resistivity which can be influenced by factors such as substrate type, epitaxy, crystal structure, and degree of oxygenation [10]–[13]. Even high-quality *c*-axis YBCO films can show some anisotropy in resistivity within the substrate plane. This may be due to sample inhomogeneity, impurity phases, twinning, heteroepitaxial growth, high-angle grain boundaries, or other variations resulting from the film growth process. In some of our Inverted Cylindrical Magnetron (ICM) sputtered films, the anisotropy was observed to be as great as 30% upon a 90° rotation of the sample. This anisotropy is reflected in the electrical characteristics of resistance ratio (*RR*), transition temperature (T_c), critical current density (J_c), and the response to small external applied magnetic fields. In patterning such samples for critical current measurements, one does not know how to account for any anisotropy on the measurement parameters. In order to relate the transport to the film morphology, thin film YBCO was deposited on (110) STO and characterized with respect to the grain orientation. In this paper, we report new results on the characteristics of the normal, superconducting, and small magnetic field properties of YBCO thin films deposited on (110) STO substrates and compare the results to those of *c*-axis YBCO films on (100) STO.

II. SAMPLE PREPARATION

The YBCO thin films used in this investigation were deposited by ICM reactive sputtering in a 1:1 argon to oxygen gas mixture and at a total pressure of 53 Pa [14]. The gas mixture was fixed by two mass flow control valves each set to a 50 sccm flow rate and the pressure maintained by throttling a gate valve ahead of a 360 l/s turbomolecular pump. A stainless steel holder on which the substrates were mounted was held at a temperature of 780 °C during deposition by radiative heating, a type K thermocouple, and a temperature controller. The 6.4 mm² (110) STO substrates were cleaned in boiling

Manuscript received May 26, 1999. This research was supported by the Office of Naval Research. The review of this paper was supervised by Editor R. S. Withers.

E. J. Cukauskas, J. M. Pond, and E. A. Dobisz are with the Naval Research Laboratory, Electronics Science and Technology Division, Washington, DC 20375 USA (e-mail: cukauskas@estd.nrl.navy.mil).

W. J. DeSisto was with the Naval Research Laboratory, Electronics Science and Technology Division, Washington, DC 20375 USA. He is now with the University of Maine, Orono, ME 04473 USA.

Publisher Item Identifier S 1051-8223(00)09749-9.

methanol and rinsed in hot isopropyl alcohol followed by drying in flowing nitrogen before mounting. Thermal contact of the substrates to the stainless steel holder was provided by silver paste and overnight drying in flowing nitrogen. Prior to inserting the holder into the ICM deposition chamber, the holder was baked at 150 °C for 20 min on a hot plate. During the deposition process, the holder temperature was monitored by the thermocouple inserted into a well in the center of the holder.

The YBCO film growth process began with outgassing the holder and substrates over a two hour period while the temperature was brought to and stabilized at 780 °C for the film growth. The YBCO target was then presputtered in the gas mixture at 135 mA dc with a shutter closed over the substrates for 10 min while the deposition rate stabilized. A 4 V dc bias was applied to the gun anode and served to ensure the collection of the electrons from the cathode (target) and any negatively charged ions. This voltage served to attenuate any negative ion bombardment of the growing YBCO film and helped to maintain the film stoichiometry. The 1 kÅ YBCO films were deposited at a rate of approximately 22 Å/min after which they were cooled to ambient temperature in one atmosphere of flowing oxygen. The films remained in the oxygen filled chamber overnight before removal.

Prior to characterization of the films, four 2 kÅ thick silver contact pads were e-beam evaporated through a shadow mask and formed a low resistance contact to the film. The contact pads were positioned at the four corners of the film. The “as deposited” films were characterized by their resistance (R) as a function of temperature (T) and their T_c . The films were then patterned into a 2.5 mm square parallel to the STO edges using standard photolithography and wet chemical etching in 10 : 1 H₂O : HCl. This square geometry, illustrated in Fig. 1, allows for selecting the current path either along the c -axis or along the basal plane for the same piece of YBCO film. The square had enough area to obtain a sufficient signal strength for the inductive microwave measurements and analysis.

III. MORPHOLOGY

The crystal structure of the YBCO films was investigated using CuK α radiation and an automated independent theta-two theta x-ray diffractometer. Scans in two theta from 20 to 80° were taken to ensure that all the major YBCO peaks were covered in the scan range. The logarithm of intensity versus two theta in the vicinity of the (110) diffraction peak is illustrated in Fig. 2 where the (110) STO and (110) YBCO are clearly visible. The (103) YBCO peak is barely visible on the high-angle side of the (110) STO peak. The (110) YBCO peak appears broad suggesting there may be an additional peak slightly higher in two theta. This peak may be due to an impurity phase or other oxide. There is also evidence (not illustrated) of the (206) and (220) YBCO peaks at higher two theta in the vicinity of 68°, however, because of their low intensity they appear on the shoulder of the larger (220) STO substrate peak. At these high angles we observed the K α splitting in the (220) STO peak. There was no evidence of any c -axis peaks over the scan range. In contrast, a two theta scan taken on a c -axis YBCO film deposited on (100) STO

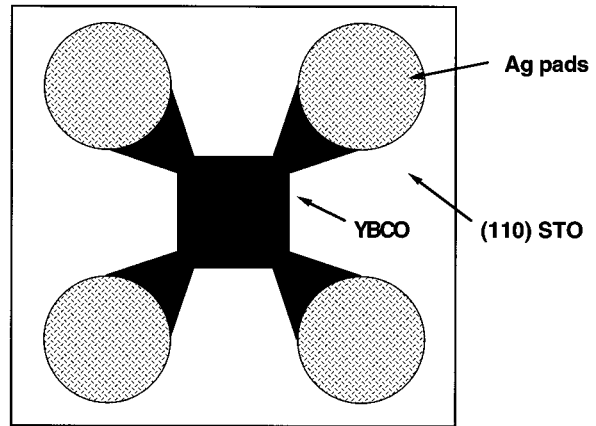


Fig. 1. Patterned film geometry used for the electrical and microwave characterization of the YBCO thin films on (110) STO substrates. The square region measures 2.5 mm on each side.

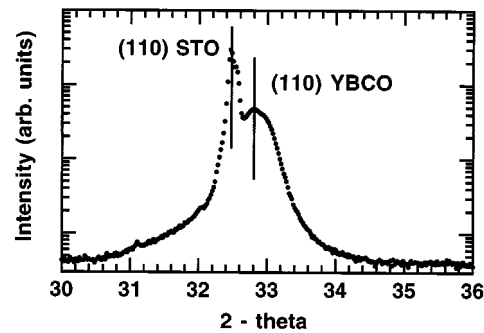


Fig. 2. X-ray diffraction intensity scan in the vicinity of the (110) YBCO and (110) STO peaks. The (103) YBCO peak appears to be on the shoulder of the STO peak.

showed predominately the (00 l) YBCO peaks with a few small impurity and the substrate peaks [14]. The c -axis lattice parameter was determined from a fit to the (00 l) peaks to be 11.69 Å indicating a well oxygenated YBCO film [15]. The insufficient number of diffraction peaks for the YBCO film deposited on the (110) STO did not allow for the accurate determination of the basal plane lattice parameters for that film orientation.

The surface morphology of the YBCO thin films was investigated using a Hitachi S-800 Scanning Electron Microscope (SEM). Fig. 3(a) illustrates the surface of a YBCO film deposited on (110) STO. The entire surface is covered with elongated grains which are aligned parallel to the substrate edge. Additionally, many of the grains appear to have small particles on their surfaces. These particles may be impurity phases or other material not incorporated into the YBCO grains and may be associated with the observed unidentified x-ray peaks. The YBCO grains are typically 1 μ m or less in length along the c -axis direction and less than 3 kÅ in width along the basal plane. The small particles on the grain surfaces are less than 300 Å in diameter. It is not known if these particles are only on the surface or also between the grains in the interior of the film. This could have a significant impact on the transport characteristics of the films. The surface morphology of a c -axis YBCO film deposited on (100) STO is illustrated in Fig. 3(b). The film surface is covered with what appears to be voids, however a closer look reveals a

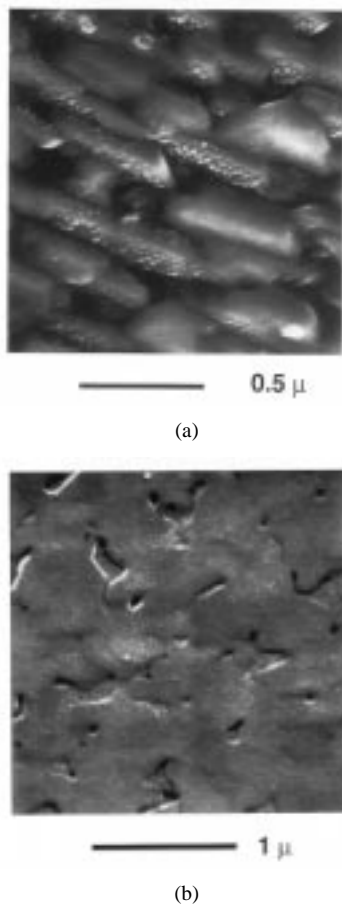


Fig. 3. Electron micrographs of the surface of a YBCO film deposited on (a) a (110) STO and (b) a (100) STO substrate. In (a), the elongated grains are aligned parallel to the substrate edge; in (b) the c -axis grain boundaries are nearly indiscernible.

YBCO film below these open regions on the surface. It is possible to minimize these open regions by changing the anode bias voltage and the dc cathode current to the ICM gun, however not always in a reproducible way. Note that grains are well connected with essentially indistinguishable grain boundaries and show no grain anisotropy in the plane of the film. There are also some small particles on the surface but not nearly as dense as those of the (110) YBCO grains. These particles may be Cu-rich precipitates observed in other *in situ* film deposition processes [16].

IV. ELECTRICAL CHARACTERIZATION

The electrical characterization of the YBCO films was performed in a closed cycle helium refrigerator equipped with a silicon diode thermometer, resistance heater, and external temperature controller for temperature stability and for setting the cooling and heating rates of the sample. Thermal contact of the sample to a small cylindrical aluminum block attached to the cooling stage was provided by thin indium foil. The sample was mounted on the aluminum block symmetric to the silicon diode thermometer. Accuracy of the thermometer was ensured by comparing the agreement of the transport measurements to those taken in another refrigerator. Agreement was found to be

within the tolerance of the silicon diode thermometers. Electrical contact to the silver pads on the film surface was made by spring loaded contacts which also served to press the sample into the indium foil ensuring that good thermal contact of the sample with the cooling stage was maintained.

The patterned YBCO films were characterized by their transition temperature, resistance ratio, and critical current (I_c) as a function of temperature and external applied magnetic field. The measurement current entered the sample through two adjacent pads and the voltage was measured at the two opposite pads. The electrical characteristics were determined for the two different orientations of the sample, one for current along the c -axis and the other for current along the basal plane. This was accomplished simply by rotating the set of IV leads by 90° (see Fig. 1). The T_c was defined as the temperature for which the film resistance became less than $0.1 \text{ m}\Omega$ and the RR was defined as the ratio of the film resistance at 295K to that at 100K. The critical current was defined as the current for which a $0.1 \mu\text{V}$ voltage developed across the voltage leads of the sample. The characteristics of the (110) YBCO were measured and compared to those of the c -axis film made on (100) STO. A summary of the “as deposited” characteristics and those of the patterned samples for each orientation is tabulated in Table I. The ratio of the high resistance to the low resistance value at 300K was calculated and listed in Table I, this gives a measure of the resistivity anisotropy of the film. Notice how the T_c of the (110) YBCO film dramatically increased after processing. This is an indication that the film may have been over-oxygenated [17]. The c -axis YBCO film was unaffected by the processing which is typical for a good film.

A. Resistance Anisotropy

The resistance as a function of temperature, $R(T)$, for the patterned (110) YBCO films was measured for each orientation. The magnitude of the resistance was such that different measurement currents were used for each orientation in order that a useful voltage developed across the film. Two adjacent pads were used for current to the film and the two opposite pads served as the voltage pads. A $10 \mu\text{A}$ current was used for current along the c -axis and 1 mA for current along the basal plane. The resistance along the c -axis direction was approximately 256Ω at 300K while along the basal plane it was about $271 \text{ m}\Omega$. This corresponds to a resistance anisotropy of 945. The T_c as defined above was 78.9K along the c -axis and 84.8K along the basal plane. The normalized resistance, $R(T)/R(300\text{K})$, for each orientation versus temperature is illustrated in Fig. 4 for the patterned (110) YBCO film. The resistance ratio is easily determined from the figure to be 1.4 for the c -axis and 9.4 for the basal plane orientations.

These results are significantly different from those of a good c -axis YBCO film. A typical c -axis YBCO film deposited by ICM sputtering on (100) STO has a T_c greater than 86K and a RR greater than 2.6, however there may still be some anisotropy observed in its properties. As an example, we observed a 22% anisotropy in the room temperature resistance of an ICM sputtered c -axis YBCO film and only a T_c difference of less than 0.3K for a film having a T_c of 87.5K. These differences can be explained by sample inhomogeneity however the resistance

TABLE I
SUMMARY OF THE ELECTRICAL PROPERTIES OF THE as-DEPOSITED AND PATTERNED YBCO FILMS ON (110) AND (100) STO

As - deposited					Patterned			
Substrate	Orientation	RR	$R_{\text{high}}/R_{\text{low}}$	T_c (K)	T_c (K)	RR	$R_{\text{high}}/R_{\text{low}}$	ΔT (20% M)
(110) STO	c-axis	1.7	75.7	60.9	78.9	1.4	945	10 K
(110) STO	basal plane	4.1		65.9	84.8	9.4		3.7 K
(100) STO	high R	2.8	1.23	87.5	87.5	2.8	1.22	1.5 K
(100) STO	low R	2.5		87.0	87.2	2.5		1.1 K

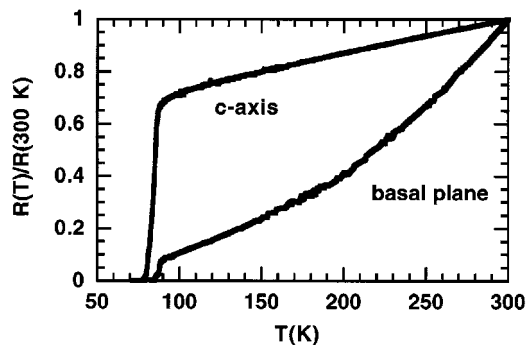


Fig. 4. Normalized resistance versus temperature along the c -axis and basal plane for a patterned (110) YBCO film. A $10 \mu\text{A}$ measurement current was used along the c -axis and 1 mA along the basal plane.

ratios of this film were 2.8 and 2.5 for two orientations of the sample. The RR is affected by factors such as oxygenation, film epitaxy, disorder, grain boundary characteristics, and other material issues all of which can also lead to inhomogenities.

B. Critical Current Anisotropy

The anisotropy in the critical current was investigated by characterizing both its magnitude and temperature dependence to gain a more thorough understanding of the transport in these YBCO films deposited on (110) STO. The characteristics of the critical current are strongly influenced by factors such as intergranular and intragranular coupling, grain orientation, stoichiometry, oxygenation, defects, and other thin film parameters [12], [18]. Equally important as the magnitude of the critical current is its temperature dependence and response to external magnetic fields. The temperature dependence of the critical current was measured along the c -axis and along the basal plane for the film whose $R(T)$ traces are illustrated in Fig. 4. The difference observed in the resistive T_c is also reflected in the T_c as determined by the zero critical current temperature for each orientation. The c -axis critical current became distinctly zero in agreement with the resistive T_c measurement. Illustrated in Fig. 5 are the temperature dependencies of the critical currents for the c -axis and basal plane orientations. Indicated on the plot are the resistive T_c points for each orientation. The analysis of the temperature dependence of the critical current along the c -axis showed a linear SIS dependence in $(1-t)$ for $t > 0.99$, where $t = T/T_c$ is the reduced temperature. At lower temperature ($t < 0.99$), the dependence became

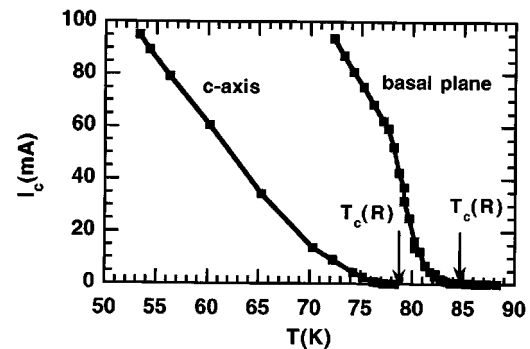


Fig. 5. Critical current versus temperature for the c -axis and basal plane orientations of the (110) YBCO patterned film. The Resistive T_c for each orientation is indicated on the plot.

quadratic indicating the intergranular coupling was SNS . The c -axis critical current characteristics are influenced by both the intergranular coupling between the grains and intragranular coupling between the planes in the unit cell. This change in intergranular coupling has been observed in other HTS materials [19]. Additionally, there may also be some intergranular coupling between adjacent grains along their adjoining basal planes, especially at the lower temperatures.

The temperature dependence of the critical current along the basal plane is distinctly different from that along the c -axis. On the linear I_c versus T plot of Fig. 5, at least three different regions are apparent. A $\log I_c$ versus $\log(1-t)$ plot reveals a low temperature region linear in $(1-t)$ followed by a quadratic-like region between $t = 0.92$ and 0.98 above which I_c again tends toward a linear dependence of $(1-t)$. It is interesting to note that this quadratic-like region for the basal plane begins at the temperature for which the c -axis critical current becomes finite. There is an apparent large anisotropy in the magnitude of I_c versus temperature, however looking at the I_c versus reduced temperature shows the large anisotropy near T_c gradually falls off to 2 for t less than 0.5. This could indicate that the intergranular coupling becomes stronger and the transport becomes more three dimensional throughout the volume of the film rather than along the direction of the grain orientation. T_c as determined by I_c becoming zero was not as clearly defined as in the case of the c -axis critical current. We observed a "zero voltage" current up to temperatures as high as 180K. This "zero voltage" current is not believed to be a real supercurrent but rather due to current redistribution. These effects have been particularly observed in

tunneling structures [20]. Because of this ambiguity in zero critical current, we used the value of T_c from the resistive transition in analyzing the critical current temperature dependence along the basal plane. This choice of T_c is also supported by the magnetic field measurements discussed in the next section.

The c -axis YBCO film on (100) STO was patterned into the same geometry as the (110) YBCO film and its I_c properties were likewise studied. Like the resistive T_c of this film, there was also an anisotropy in the critical current with sample orientation. Here, the critical current in the higher T_c orientation was a factor of two greater than the critical current in the lower T_c orientation. This anisotropy in I_c is large close to T_c and rapidly approaches 2 at a reduced temperature of $t = 0.99$. It is interesting that the anisotropy in I_c approaches 2 for both the (110) and the c -axis YBCO films only much more rapidly for the c -axis film. The temperature dependence of the critical current shows the same Ginzburg–Landau $(1 - t)^{3/2}$ dependence for both orientations. The difference in the anisotropy of I_c is too great to be due solely to the difference in T_c and sample geometric differences and could be due to the existence of some other YBCO orientation or phase.

C. Magnetic Field Effects

The response of the critical current to small external applied magnetic fields was investigated for the YBCO on (110) STO and compared to that of the c -axis YBCO film. This characterization can give some insight into the potential usefulness of these films for vortex flow device development. Magnetic fields up to 170 G were applied perpendicular to the surface of the films by a solenoid magnet positioned with the sample at its center. Higher fields resulted in radiatively heating of the cold stage by the Joule heating of the copper magnet windings. The multi-turn magnet was wound on a hollow copper form which had a length to diameter ratio of two. The magnet was positioned in the vacuum space between the cold stage and vacuum wall of the refrigerator. The magnet form was heat sunk to the refrigerator’s removable top plate and cooled by forced air over radiation fins attached to the plate.

There were significant differences in the response of the critical current to the external magnetic fields for each orientation of the YBCO film on (110) STO. The response was defined as the fractional change or “modulation” (M) of the critical current for an applied magnetic field (B) and given by the equation: $M(B) = (I_c(0G) - I_c(B))/I_c(0G)$, where $I_c(0G)$ is the critical current in zero applied field and $I_c(B)$ is the critical current in a field of B . For this study, an applied field of 25 G was used to characterize the temperature dependence of the modulation for each orientation. The modulation for the basal plane orientation was negative meaning that the critical current increased with the applied 25 G field. This could be an indication that there were Josephson vortices trapped or Abrikosov vortices pinned along the basal planes which decreased in density with the application of the applied field. For a given temperature, the magnitude of the modulation increased with field reaching a maximum at approximately 50 G after which it decreased and finally became positive above 100 G. This supports the idea of the existence and

movement of vortices within the film. However for the c -axis orientation, the modulation was positive and I_c decreased with magnetic field. We define a useable level of field modulation to be a 20% change in I_c for a 25 G field. For the basal plane orientation there was approximately a 3.7K temperature range where the magnitude of the modulation was at least 0.2, however for the c -axis orientation, the temperature range was greater than 10K. The useable temperature range is listed in Table I as $\Delta T(20\%M)$. This useable temperature range impacts the potential use of these films for device development. The modulation for each orientation is illustrated in Fig. 6. Also shown are the 20% modulation temperature and the resistive T_c for each orientation. Above T_c , the modulation was zero and the greatest modulation magnitude was very close but below T_c . The lack of any significant modulation above T_c for the basal plane orientation is compatible with the “zero voltage” current above T_c not being superconducting in origin.

The modulation for the c -axis YBCO film showed positive modulation for both orientations with the 20% modulation at approximately 1.1–1.5K below T_c for a 25 G field. This temperature range over which large modulation occurred increased with increasing field as expected. The small difference in the modulation between the two orientations is probably associated with the small anisotropy in the $R(T)$, T_c , and $I_c(T)$ characteristics. YBCO thin films on (100) STO show little potential for applications in vortex flow device development whereas YBCO on (110) STO shows significant promise for the in plane c -axis oriented grains. However, c -axis films have been used in vortex flow devices after arrays of parallel bicrystal grain boundary junctions have been fabricated into them [18]. These devices have demonstrated the feasibility of fabricating three terminal superconducting devices having gain for applications in superconducting electronics.

D. Microwave Measurements

Inductive measurements for the two sample orientations were made using a broadband microwave technique [21]. The sample was mounted on the cold finger of a different, although similarly instrumented, two-stage closed-cycle refrigerator. A magnetic field probe (very small loop antenna) fabricated from very thin diameter coaxial cable was fixed in close proximity to the sample. The other end of the coaxial cable was connected to a Hewlett Packard 8510C microwave vector network analyzer. Throughout the measurement frequency range, 50 MHz–5 GHz, the magnetic field probe is very small compared to the wavelength. Hence, the microwave field in the vicinity of the loop is primarily a reactive magnetic field resulting in the vast majority of the incident microwave energy being reflected. The phase of the reflected signal, in reference to the incident signal, is a measure of the reactive near field of the loop. As the sample is cooled through the transition, the magnetic field is expelled from the sample as superconducting image currents are induced in the film changing the spatial distribution of the magnetic field of the loop probe. Since the loop is very small compared to wavelength, to first order the phase of the reflected signal is 180°. The resultant change in the relative phase of the reflected signal

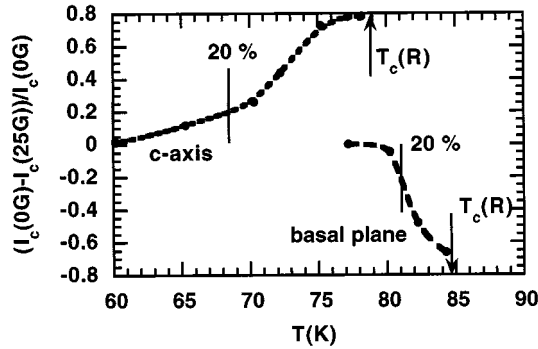


Fig. 6. Critical current modulation for each orientation as a function of temperature due to a 25 G applied magnetic field. Indicated are the resistive T_c and 20% modulation temperatures for each orientation.

is recorded versus temperature. The microwave reflection coefficient, S_{11} , is given by

$$S_{11} = \frac{R_{lp} + j\omega L_{lp} - Z_0}{R_{lp} + j\omega L_{lp} + Z_0} \quad (1)$$

where Z_0 is the characteristic impedance, 50Ω , of the coaxial cable system and where the loop is modeled as a series combination of an inductor L_{lp} and a resistor R_{lp} at an angular frequency of ω . For frequencies where the loop impedance is small, the phase angle of S_{11} is

$$\theta = \pi - 0.04\omega L_{lp}(1 + 0.04R_{lp}). \quad (2)$$

Hence, as flux is incrementally expelled from regions of the sample the measured inductance is changed proportionately. The microwave reflection coefficient was measured at several frequencies while the sample was cooled in each orientation. This results in approximately ten measurements per degree at each of seven discrete frequencies in the 0.05–5.0 GHz range. In addition, a four-point resistance measurement using the four silver contact pads was made simultaneously with the microwave measurement. Instrumentation for this measurement was a standard digital multimeter with 4-wire resistance capabilities. This was done to provide a reference to the more accurate four-point measurements performed in the other cryogenic system.

In order to examine the anisotropic transport properties of the film the loop was chosen to have a large (~ 5) length to width ratio as illustrated in Fig. 7, in contrast to a more conventional circularly symmetric loop probe. This large length to width ratio ensures that a much greater percentage of the induced image currents flow parallel to the axis of the coaxial cable. By arranging the axis of the coaxial cable along the c -axis grains during the first measurement and along the basal plane in a subsequent measurement, the anisotropy of the HTS film can be examined independent of the contact metallization and independent of any current percolation path due to film inhomogeneities. Thus, this inductive measurement can be used to corroborate the anisotropic nature of transport along the c -axis as compared to the basal plane transport properties as being an intrinsic property of the film. Fig. 7 illustrates the c -axis grains aligned with the axis of the coaxial cable center conductor. Due to the highly directional shape of the loop probe, the majority of the induced

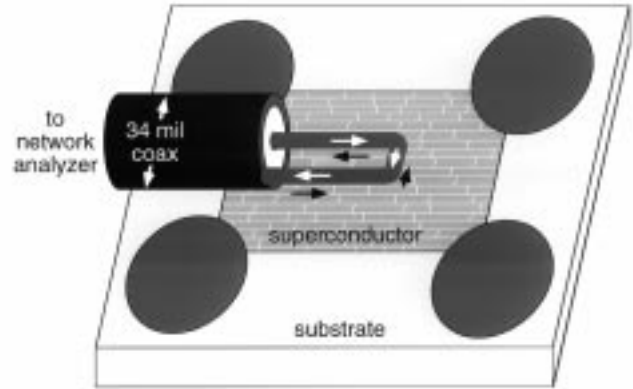


Fig. 7. Placement of the high aspect ratio loop probe positioned so that the majority of the induced image current (black arrows) flows in the direction of c -axis.

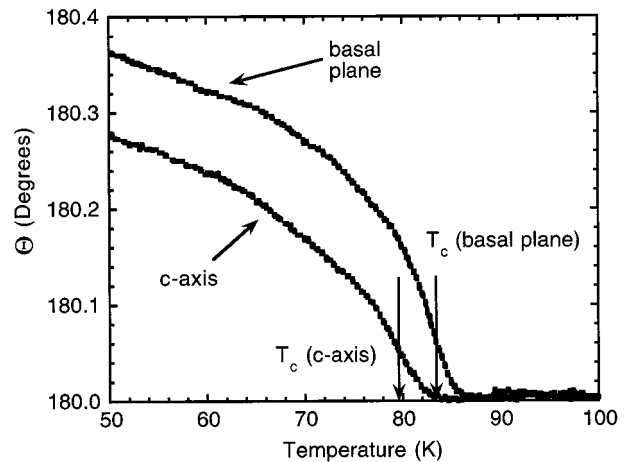


Fig. 8. Phase of S_{11} for the inductive measurements at 0.5 GHz for each sample orientation. The T_c of the corresponding resistive transitions is indicated for reference.

image current, illustrated by the dark arrows, flows along the c -axis grain direction with relatively little current flowing in the direction of the basal plane. When the sample is rotated 90° with respect to the coaxial cable center conductor, the opposite is true.

The measurement of the microwave inductance aligned along the c -axis grains is compared with that aligned along the basal plane in Fig. 8. The resistive T_c point for each orientation is also indicated in the figure. As can be seen the difference in the transition temperatures as inferred from the resistance measurements between the two orientations correlates well with the earlier resistance measurements. The microwave inductance measurement exhibits almost exactly the same difference in transition temperature as the resistance measurement. The onset of the microwave inductance transition although higher than the resistive T_c , has been consistently seen to correlate well with the “zero-resistance” T_c [21]. The discrepancy in the data of Fig. 8 may be associated with the measurement current of the multimeter used for the resistive measurements. Since the change in phase of the reflected signal is proportional to the change in

inductance which, in turn, is proportional to the flux being expelled, this measurement confirms that the anisotropy is homogeneous within a region of the film on the order of the area of the loop. Similar measurements were made on the *c*-axis film and showed no significant difference in the microwave inductance for the two orientations.

V. SUMMARY AND CONCLUSIONS

We have investigated and compared the morphology and electrical properties of ICM sputter deposited YBCO on (110) and (100) STO substrates. The films deposited on (110) STO showed only the (110) and (103) diffraction peaks while those on (100) STO were highly *c*-axis oriented showing only the (00 ℓ) diffraction peaks. SEM micrographs showed the (110) films to consist of elongated grains parallel to the substrate edge while the *c*-axis films showed a surface of tightly coupled grains with nearly indiscernible grain boundaries. The films were patterned into small squares parallel to the substrate edges with the electrical contact pads located at the four corners. This geometry allowed for the measurement currents to be directed perpendicular or parallel to the *c*-axis of the grains for the same volume of YBCO film.

The resistive anisotropy of the (110) YBCO film was determined to be 945 : 1 with the *c*-axis orientation having the higher resistance. The resistance ratio was 1.4 for the *c*-axis and 9.4 for the basal plane orientations, respectively. T_c for the two orientations differed significantly with 78.9K for measurement along the *c*-axis grains and 84.8K for measurement along the basal plane. T_c also dramatically increased by as much as 19K after patterning and etching which is associated with the loss of excess oxygen. In comparison, the *c*-axis film on (100) STO showed only 0.3K difference in T_c and RR of 2.5 and 2.8 for the two orientations and was essentially unchanged after processing. This difference in characteristics for the *c*-axis film is attributed to sample inhomogeneity and impurity phases and/or some in plane *a*-axis grains, however the volume of any impurity phases was too small to be detected by x-ray diffraction. Agreement with these results and the microwave inductance measurements at 0.5 GHz for both films was observed for each orientation.

The critical currents of both the (110) YBCO and the *c*-axis films showed a difference of approximately two in magnitude between the two orientations. However, for the YBCO on the (110) STO, there was a significant difference in the temperature dependence for each orientation. For currents along the *c*-axis, the critical current was quadratic-like except very close to T_c where it became linear in $(1 - t)$. Along the basal planes, I_c was linear at low temperature and very close to T_c with a quadratic-like region connecting the two. The linear dependence in the low temperature region for the basal plane orientation began at the temperature coincident with the *c*-axis grain T_c . Additionally for the basal plane orientation, there was a zero voltage current at temperatures as high as 180K which is nonsuperconducting in nature. In contrast, the *c*-axis film on (100) STO showed an I_c anisotropy of two between the two orientations, however the temperature dependence was the same Ginzburg–Landau $(1 - t)^{3/2}$ dependence expected for

a *c*-axis YBCO film. The reduction of the I_c anisotropy at reduced temperature for both films suggests that the intergranular coupling becomes stronger and the transport is governed by the material throughout the volume of the film.

The magnetic field properties of the (110) YBCO were very different for each orientation. For the *c*-axis orientation, a useful (20%) critical current change was realized for up to 10K below T_c while along the basal plane, the same degree of change only had a range of 3.7K. The same degree of change for the *c*-axis film on (100) STO had a range of 1.1–1.5K. The application of a small magnetic field for the *c*-axis orientation resulted in a reduction in I_c while for the basal plane orientation, the field caused an increase in I_c . This observation for the basal plane orientation suggests the existence of Josephson and/or Abrikosov vortices between the basal planes. The ease in movement of these vortices is a measure of the potential usefulness of these films for vortex flow devices.

ACKNOWLEDGMENT

The authors would like to thank R. A. Bayles for the use of his SEM facility and B. Gorman for his help in the preparation of the figures.

REFERENCES

- [1] J. Jorgensen, B. Veal, W. Kwok, G. Crabtree, A. Umezawa, L. Norwicki, and A. Paulikas, "Structural and superconducting properties of orthorhombic and tetragonal $\text{YBa}_2\text{Cu}_3\text{O}_{7-x}$: The effect of oxygen stoichiometry and ordering on superconductivity," *Phys. Rev. B*, vol. 36, no. 10, pp. 5731–5734, Oct. 1987.
- [2] M. Beasley, "High-temperature superconductive thin films," *Proc. IEEE*, vol. 77, pp. 1155–1163, Aug. 1989.
- [3] E. J. Cukauskas, L. H. Allen, G. K. Sherrill, R. T. Holm, and C. Vold, "Morphology and transport of $\text{YBa}_2\text{Cu}_3\text{Y}_{7-x}$ sputtered in argon, oxygen, and hydrogen: Dependence on deposition temperature," *J. Appl. Phys.*, vol. 74, no. 11, pp. 6780–6787, Dec. 1993.
- [4] J. Aponte, H. C. Abache, A. Sa-Neto, and M. Octavio, "Temperature dependence of the critical current in high- T_c superconductors," *Phys. Rev. B*, vol. 39, no. 4, pp. 2233–2237, Feb. 1989.
- [5] J. De Vries, G. Stollman, and M. Gijs, "Analysis of the critical current density in high- T_c superconducting films," *Physica C*, vol. 157, pp. 406–414, 1989.
- [6] S. Ogale, D. Dijkkamp, T. Venkatesan, X. Wu, and A. Inam, "Current transport in high- T_c polycrystalline films of Y-Ba-Cu-O ," *Phys. Rev. B*, vol. 36, no. 13, pp. 7210–7213, Nov. 1987.
- [7] A. Barone and G. Paterno, *Physics and Applications of the Josephson Effect*. New York: Wiley, 1982, ch. 7.
- [8] S. Yamamoto, A. Kawaguchi, and S. Oda, "Anomalous current–voltage characteristics along the *c*-axis in YBaCuO thin films prepared by MOCVD and AFM lithography," *Physica C*, vol. 293, pp. 244–248, 1997.
- [9] K. Tanabe, Y. Hidaka, S. Karimoto, and M. Suzuki, "Observation of both pair and quasiparticle tunneling in intrinsic junction stacks fabricated on $\text{Bi}_2\text{Sr}_2\text{CaCu}_2\text{O}_{8+\delta}$ single crystals," *Phys. Rev. B*, vol. 53, no. 14, pp. 9348–9352, Apr. 1996.
- [10] S. W. Tozer, A. W. Kleinsasser, T. Penney, D. Kaiser, and F. Holtzberg, "Measurement of anisotropic resistivity and Hall constant for single-crystal $\text{YBa}_2\text{Cu}_3\text{O}_{7-x}$," *Phys. Rev. Lett.*, vol. 59, no. 15, pp. 1768–1771, Oct. 1987.
- [11] T. Ito, H. Takagi, S. Ishibashi, T. Ido, and S. Uchida, "Normal-state conductivity between CuO_2 planes in copper oxide superconductors," *Nature*, vol. 350, pp. 596–598, Apr. 1991.
- [12] C. B. Eom, A. F. Marshall, Y. Suzuki, T. H. Geballe, B. Boyer, R. F. W. Pease, R. B. van Dover, and J. M. Phillips, "Growth mechanisms and properties of 90° grain boundaries in $\text{YBa}_2\text{Cu}_3\text{O}_7$ thin films," *Phys. Rev. B*, vol. 46, no. 18, pp. 11 902–11 913, Nov. 1992.
- [13] J. P. Zheng, S. Y. Dong, D. Bhattacharya, and H. S. Kwok, "Structural and electrical properties of $\text{YBa}_2\text{Cu}_3\text{O}_{7-x}$ films on SrTiO_3 (110) substrates," *J. Appl. Phys.*, vol. 70, no. 11, pp. 7167–7169, Dec. 1991.

- [14] L. H. Allen, E. J. Cukauskas, and M. A. Fisher, "Thin film composites of Au and $\text{YBa}_2\text{Cu}_3\text{O}_{7-\delta}$," *Appl. Phys. Lett.*, vol. 66, no. 8, pp. 1003–1005, Feb. 1995.
- [15] R. J. Cava, B. Batlogg, C. H. Chen, E. A. Rietman, S. M. Zahurak, and D. Werder, "Single-phase 60-K bulk superconductor in annealed $\text{Ba}_2\text{YCu}_3\text{O}_{7-\delta}$ ($0.3 < \delta < 0.4$) with correlated oxygen vacancies in the Cu–O chains," *Phys. Rev. B*, vol. 36, no. 10, pp. 5719–5722, Oct. 1987.
- [16] Z. Han, T. I. Selinder, and U. Helmersson, "Formation of Cu-rich particles on the surface of $\text{YBa}_2\text{Cu}_3\text{O}_{7-x}$ thin film grown by *in situ* off-axis sputtering," *J. Appl. Phys.*, vol. 75, no. 4, pp. 2020–2025, Feb. 1994.
- [17] J. R. Gavaler, J. Talvacchio, and R. W. Weinert, "Effect of oxygen over-doping on T_c and R_s of YBCO films," *IEEE Trans. Appl. Supercond.*, vol. 5, pp. 1173–1176, June 1995.
- [18] R. Gerdemann, L. Alff, A. Beck, O. M. Froehlich, B. Mayer, and R. Gross, "Josephson vortex-flow transistors based on parallel arrays of $\text{YBa}_2\text{Cu}_3\text{O}_{7-\delta}$ bicrystal grain boundary junctions," *IEEE Trans. Appl. Supercond.*, vol. 5, pp. 3292–3295, June 1995.
- [19] E. J. Cukauskas and L. H. Allen, "Critical current characteristics of composite thin films of Au and $\text{YBa}_2\text{Cu}_3\text{O}_7$," *Physica C*, vol. 313, pp. 11–20, 1999.
- [20] R. J. Pedersen and F. L. Vernon, "Effect of film resistance on low-impedance tunneling measurements," *Appl. Phys. Lett.*, vol. 10, no. 1, pp. 29–31, Jan. 1967.
- [21] J. M. Pond, L. H. Allen, and E. J. Cukauskas, "A simple technique for measuring the transition temperature at microwave frequencies," *IEEE Trans. Appl. Supercond.*, vol. 7, pp. 1857–1860, June 1997.



Edward J. Cukauskas received the B.S. and M.A. degrees in physics from the University of Scranton, Scranton, PA, and the Ph.D. degree in physics from the University of Virginia, Charlottesville, in 1968, 1970, and 1974, respectively.

In 1977, he joined the Naval Research Laboratory, Washington, DC, as a research physicist working in the area of superconductive materials and devices. Since the advent of high-temperature superconductivity, he has been investigating YBCO thin film materials deposited by reactive sputtering

techniques. His current research interests also include materials research of sputter deposited ferroelectric thin films for microwave device development.



Jeffrey M. Pond (M'82) received the B.S.E.E. degree from Michigan State University, East Lansing, in 1978 and the M.S. and Ph.D. degrees in electrical engineering from the University of Michigan, Ann Arbor, in 1979 and 1982, respectively.

In September 1982, he joined the Microwave Technology Branch of the Naval Research Laboratory, Washington, DC. His research interests have included microwave cryogenic measurements and electronics, and microwave measurements and applications of superconductors and ferroelectrics.

His current research focus is on novel microwave resonator and filter concepts.

Dr. Pond has been active on both the Technical Program Committees and Steering Committees of recent International Microwave Symposia. Since January 1999, he has been Webmaster for MTT-S and is currently serving as MTT-S Secretary.



Elizabeth A. Dobisz received the B.S. and M.Eng. degrees in engineering physics from Cornell University, Ithaca, NY, in 1975 and 1976, respectively, and the Ph.D. degree in materials science from University of Wisconsin (CITY?) in 1985.

Currently, she is in the Electronics Science and Technology Division of the Naval Research Laboratory, Washington, DC. Her interests are in the areas of electron beam and proximal probe lithographies, nanofabrication, materials processing and analysis, and surface modification through self

assembled monolayers.

Dr. Dobisz received the NRL Edison Patent Award, for a patent on apparatus for proximal probe lithography, in 1997. In 2000, she received the National Women in Science and Engineering Award for Scientific Achievement. She has been active in the American Vacuum Society (National Symposium Vice Chair in 1997, Web Committee Chair (1997–2000), and Director (1998–1999)), the SPIE Symposium on Electron, X-ray, EUV, and Ion-Beam Submicrometer Lithographies (Symposium Chair 2000 and 2001), and the International Conference on Electron, Ion, and Photon Beam Technology and Nanofabrication (Section Head, 1994–2000).



William J. DeSisto He is currently an Assistant Professor of chemical engineering at the University of Maine, Orono. From 1989 to 1999, he worked full-time at the Naval Research Laboratory, Washington, DC. His major area of interest is in the field of MOCVD of complex oxides for electronic and sensing applications. He has authored or coauthored 24 papers in refereed journals, has given six invited and 19 contributed oral presentations, and has one patent. His recent achievements include the development of an *in-situ* sensor for solid source delivery

control during complex oxide MOCVD. His current interests include ceramic membrane synthesis, magnetic material synthesis, and the development of new *in-situ* process sensors for monitoring and controlling the surface and near surface chemistry during MOCVD of complex oxides.